PNAS

Supporting Information for:

Early Human Collective Practices and Symbolism in The Early Upper Paleolithic of Southwest Asia

Omry Barzilai*, Ofer Marder, José-Miguel Tejero, Avner Ayalon, Miryam Bar-Matthews, Talia Abulafia, Ron Lavi, Mae Goder-Goldberger, Maayan Shemer, Lotan Edeltin, Alexander Wiegmann, Amos Frumkin, Avshalom Karasik, Gal Yasur, Reuven Yeshurun, Irit Zohar, Francesco Berna, Mark Hans, Jerold S. Goldberg, Yvonne McDermott, Linda Spurlock, Ariel Pokhojaev, Waseem Habashi, Hila May, Rachel Sarig, and Israel Hershkovitz*

* Omry Barzilai

obarzilai@univ.haifa.ac.il

* Israel Hershkovitz

anatom2@tauex.tau.ac.il

This PDF file includes:

Other supporting materials for this manuscript include the following:

- Movie: The ritual compound and the engraved boulder from Manot Cave (3D reconstruction).

1. Rock engravings and permanent art objects: A brief review

Prehistoric engravings featuring abstract, composite, and naturalistic depictions have been discovered globally on diverse objects, including bones, boulders, stone slabs, and pebbles (e.g.,(1-14)). These engravings are commonly linked to symbolic activities (e.g.,(15-23)).

Middle Paleolithic: While there is some earlier evidence of engravings on portable objects in the late Lower Paleolithic (13, 24-26), it was only during the Middle Paleolithic (MP) in Eurasia and the Middle Stone Age (MSA) in Africa that this phenomenon became constant (27). Well-recognized MSA engravings are those found in Blombos Cave, dated to ca. 100-75 ka (18, 28-30).

The engravings at Blombos Cave, crafted on ochre slabs, exhibit abstract geometric designs, including lines, cross-hatched, crisscross, and ladder-like patterns. Similar engravings on ochre slabs are also identified in other MSA sites at Klasies River Cave 1, Pinnacle Point, and Klein Kliphuis (27, 31, 32). The oldest known Levantine MP engraving is a Levallois flint core featuring incised parallel lines on its cortical face, dating back to ca. 100 ka from Qafzeh Cave (33). The tradition of incorporating abstract geometric designs on flint cores and slabs persisted into the late MP period. This is evident in a Levallois core discovered at Manot Cave, featuring radiating fan-shaped incised lines (34), and a flint slab from Quneitra displaying an incised concentric pattern (12, 35). Recently, engraved bones were recovered at the MP sites of Quneitra (36), and Nesher Ramla (37). In Europe, rock engraving from MP contexts, characterized by sequential incisions, has been documented in Iberia, southwest France, the Balkans, and Crimea (16, 38, 39). Notably, among these European engravings is a crisscross pattern etched onto the bedrock at Gorham's Cave, Gibraltar (40).

Upper Paleolithic: A plethora of art objects and symbolic expressions emerge in the Upper Paleolithic (UP)(41), particularly within the archeological cultures of Europe (2, 15, 42, 43). It is believed that both parietal (on cave walls) and mobile art served as common mediums for expressing a sophisticated symbolic world, where a predominant emphasis on animals played a central role (44-46). However, non-figurative images, often referred to as “abstract motifs” or geometric signs, are abundant across numerous sites (2). The distribution of these signs along the Upper Paleolithic timeline shows regional

variability (2, 43, 47, 48). Although human images are relatively scarce in comparison to depictions of animals (49), they stand out as a notable theme in Paleolithic art (50).

Complexity of UP iconography: The iconography of the European UP is undeniably more complex than that of the Middle Stone Age/ Middle Paleolithic (MSA/MP) (43, 51). It incorporates complex geometric patterns and naturalistic depictions, predominantly featuring animals on cave walls, carved figurines, and small mobile objects (1, 52). Rock engravings were integrated into many cave paintings and onto boulders (53-55) (refer to Figs. 11-14; 20; 23; 37 in (56).

Recent discoveries of cave art expressions and portable engraved objects reported in Sulawesi, Indonesia, demonstrate that this phenomenon has extended beyond Europe to the islands of Southeast Asia (8, 57, 58). Albeit the Levantine UP cultures were significantly less rich with art expressions and exhibited only sporadic mobile engraved stone objects, such as an incised stone palette with an abstract representation of a horse from Hayonim Cave (59-61), some of them were specified as unique regional marker (62).

The recovery of a large permanent art object within the deepest zone of Manot Cave, Israel, holds the potential for expanding our understanding of social complexity and communal rituals during the Levantine UP. It can contribute to our knowledge of ancient human behavior, cultural practices, and the development of symbolic expression within this region.

2. Manot Cave and its spatial organization

Manot Cave is a unique relict karst cave located in Western Galilee, Israel. The cave (33.03ºN/35.19ºE) is situated at an elevation of about 220 m asl, nine km east of the current Mediterranean coastline. Presently, the area is characterized by a Mediterranean climate, with hot and dry summers and cool and wet winters. The average annual precipitation is ~600-700 mm/yr. The cave was formed prior to the last uplift (Pleistocene) of the region. The smooth walls, solution cupolas, and chimneys in the cave are typical of phreatic caves that formed below the water table by slow-moving water (63, 64). The cave was inhabited from the Late Middle Paleolithic through the Early Upper Paleolithic periods until its main entrance collapsed approximately 30,000 years ago.

The cave consists of an elongated main hall (80m long, 10-25m wide) and two side chambers (northern and southern chambers; Fig. S1). The topography of the main hall features a steep talus inclining from the original entrance of the cave to the center (Western talus); a deep chamber with a leveled area at its lowermost point, and a smaller talus inclining from the eastern end of the cave (Eastern talus; Fig. S1).

So far, ten archaeological layers have been defined within the primary area of domestic activity (Area E) based on well-persevered artifact deposition in direct association with intact combustion features (65, 66) (Fig. S2).

Figure S1: ***The three major excavation areas of Manot Cave.***

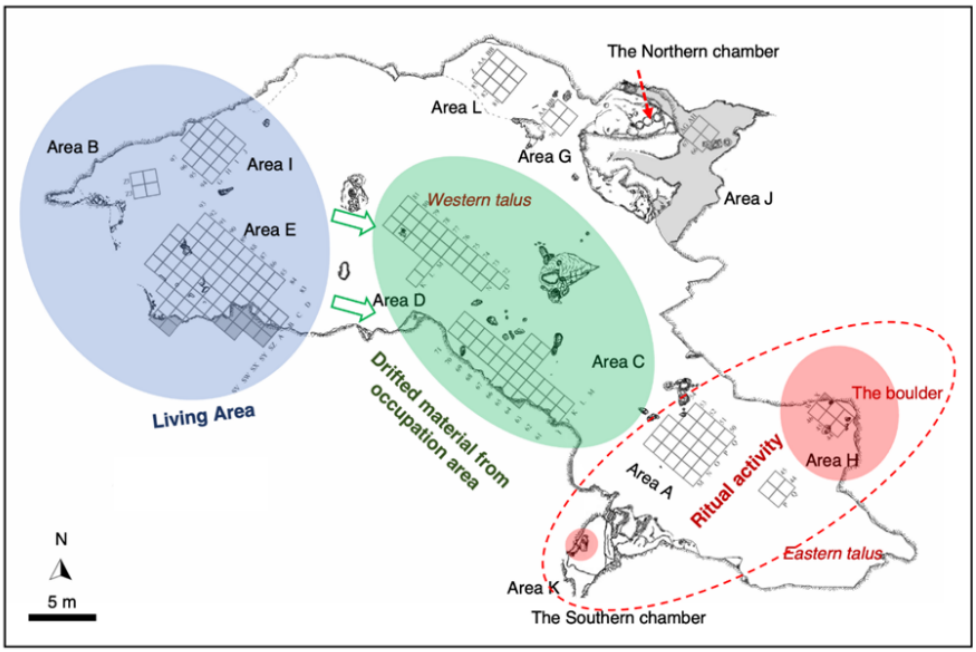

The living area (Area E; blue circle), the highest area of the cave, is connected to the ritual compound (red circle), the lowest area of the cave (a 30 m difference), by a sharply inclined talus (green circle) formed by drifted material from the living area.

These layers were attributed primarily to the Levantine Aurignacian and Atlitian cultural entities. The Levantine Aurignacian layers (Fig. S2, layers IV-VIII), which are suggested here as relating to the engraved boulder, were recently dated to ca. 37.5-36.0 ka cal BP (67). The Levantine Aurignacian material culture at Manot Cave consists of distinct lithic assemblages, including Aurignacian blades and carinated components in which frontal carination dominates. In addition, it includes rich osseous industries and personal ornaments, including incised scapulae, polished-tooth pendants, perforated

marine shells, bone awls, and antler projectile points that bear close similarity to components of the early west European Aurignacian techno-complex (68). Therefore, the archaeological record of Manot Cave supports a scenario in which a foreign band of hunter-gatherers arrived in the southern Levant ca. 38 ka cal BP, bringing with them traditions and ideas that disappeared a few millennia later (66-69). The younger, Atlitian occupation levels (Fig. S2, layers I-III) yielded minimum ages ca. 34.5-33.1 ka cal BP (67).

Figure S2. ***Occupational layers in Area E, Manot Cave (close to the original entrance).***

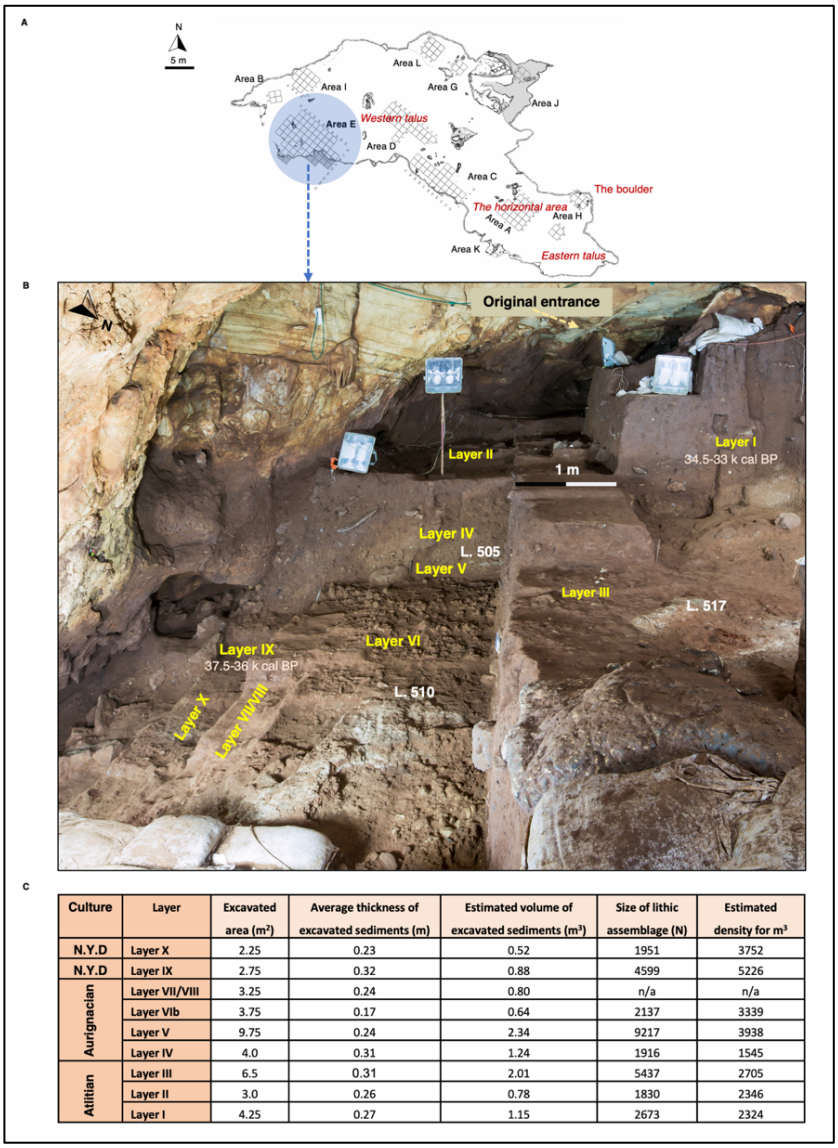

C

Culture	Layer	Excavated area (m^2)	Average thickness of excavated sediments (m)	Estimated volume of excavated sediments (m^3)	Size of lithic assemblage (N)	Estimated density for m^3
N.Y.D	Layer X	2.25	0.23	0.52	1951	3752
N.Y.D	Layer IX	2.75	0.32	0.88	4599	5226
Aurignacian	Layer VII/VIII	3.25	0.24	0.80	n/a	n/a
	Layer VIb	3.75	0.17	0.64	2137	3339
	Layer V	9.75	0.24	2.34	9217	3938
	Layer IV	4.0	0.31	1.24	1916	1545
Atlitian	Layer III	6.5	0.31	2.01	5437	2705
	Layer II	3.0	0.26	0.78	1830	2346
	Layer I	4.25	0.27	1.15	2673	2324

A. *Location of Area E at the entrance of Manot Cave (blue circle);* ***B.*** *Ten archeological layers (I-X) identified at Area E. Loci 517, 510, and 505 denote the location of hearths.* ***C****. Table summarizing the size of each excavated layer and the estimated flint density (per 1m^3). N.Y.D=culture not yet defined*

Additional evidence for *in situ* domestic activity was recorded in the adjacent Area I, located at the top of the western talus, near the north wall of the cave. Five archaeological layers, tentatively ascribed to the Levantine Aurignacian and the Atlitian, were defined there following the identification of intact combustion features, dense lithic concentration, and few faunal remains (65, 66, 70).

The western talus extends from the occupational area to a row of speleothems at the entrance to the deep chamber (Fig. S1, S3). It is composed of sediments that drift from the occupational area of the cave while containing artifacts and cave deposits (stalagmites and flowstone surfaces; Area C). The western talus inclines towards the east at an angle of approximately 20 degrees (65). Area C is extremely rich in finds and includes, charcoal flecks, flint, and faunal assemblages (71-73), as well as human remains (74). Despite its aggregation of secondary depositions, it was indicated by radiocarbon (75) and by lithic analysis (73), that the accumulation in Area C was in chronological order, namely, Early Ahmarian deposits overlaid by Levantine Aurignacian deposits.

The deep part of the cave is separated from the western talus by a row of stalagmites (Fig. S1). It comprises a leveled area at the center of the chamber, which is the lowest part of the cave (Fig S3). The deep part of the cave consists of a lofty and spacy chamber and displays a dome-like ceiling. Its huge volume (1760 cubic meters) provides good acoustics. This area is bordered by a small talus extending over 5-7 m from the eastern part of the cave. Despite surveying and test excavations, the deep part of the cave showed no evidence of domestic activities.

Area H – The engraved boulder

Excavation in the area surrounding the engraved boulder (Area H) resulted in a scarcity of artifacts. Nevertheless, numerous angular and flat stones of diverse sizes were uncovered during the excavation. A thorough inspection of these stones revealed no indications of grooves, whether natural or artificial.

Figure S3. ***The ritual compound and the corridor of stalagmites on the western talus leading to it.***

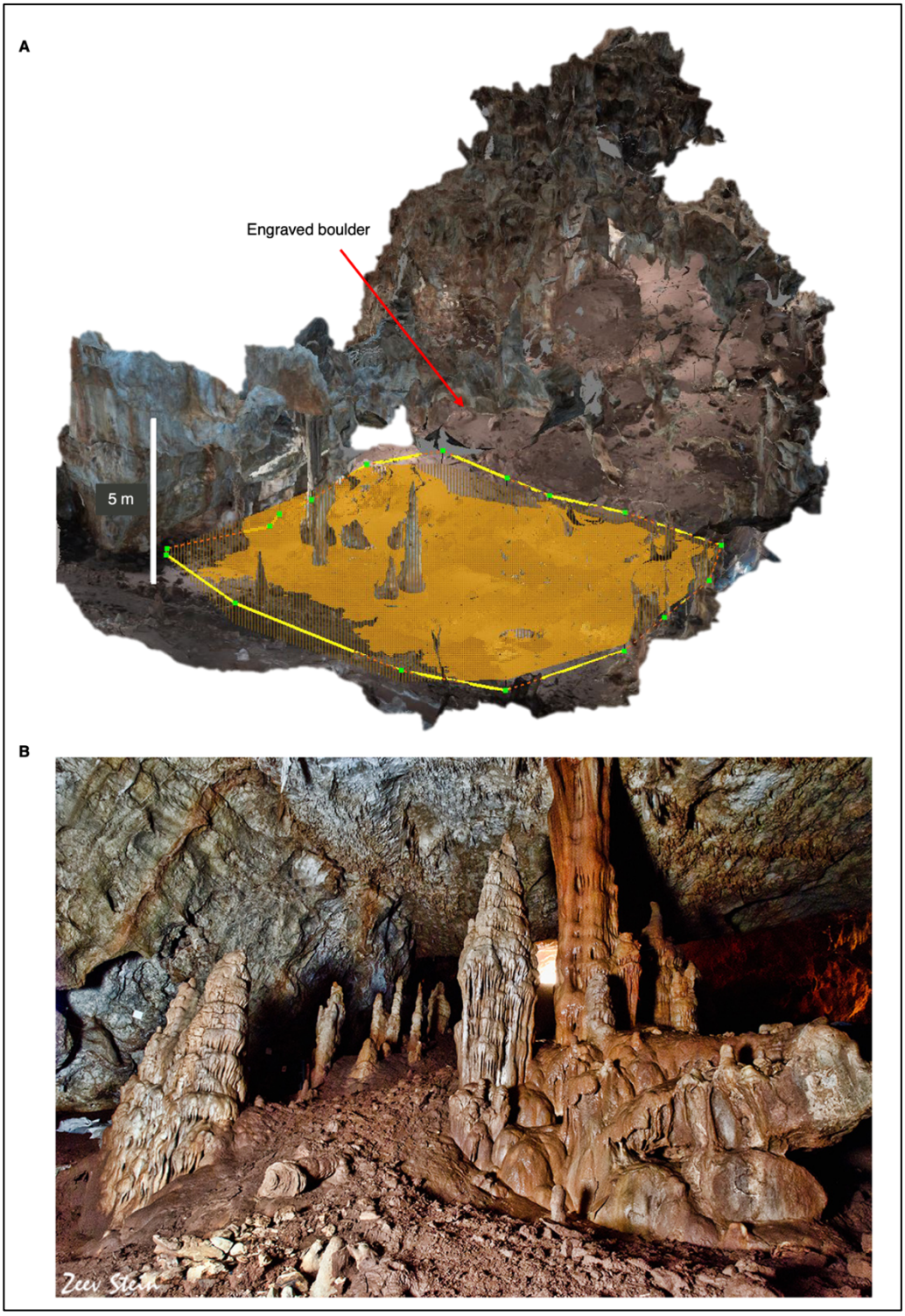

A. *A 3D model of the ritual compound and the location of the engraved boulder (red arrow). The ritual compound (orange) is a flat area located at the deepest part of the cave;* ***B.*** *A row of stalagmites located on the western talus forms a kind of corridor leading to the ritual compound.*

Figure S4. The "hidden chamber" opposite the ritual compound where the antler was found (Area K).

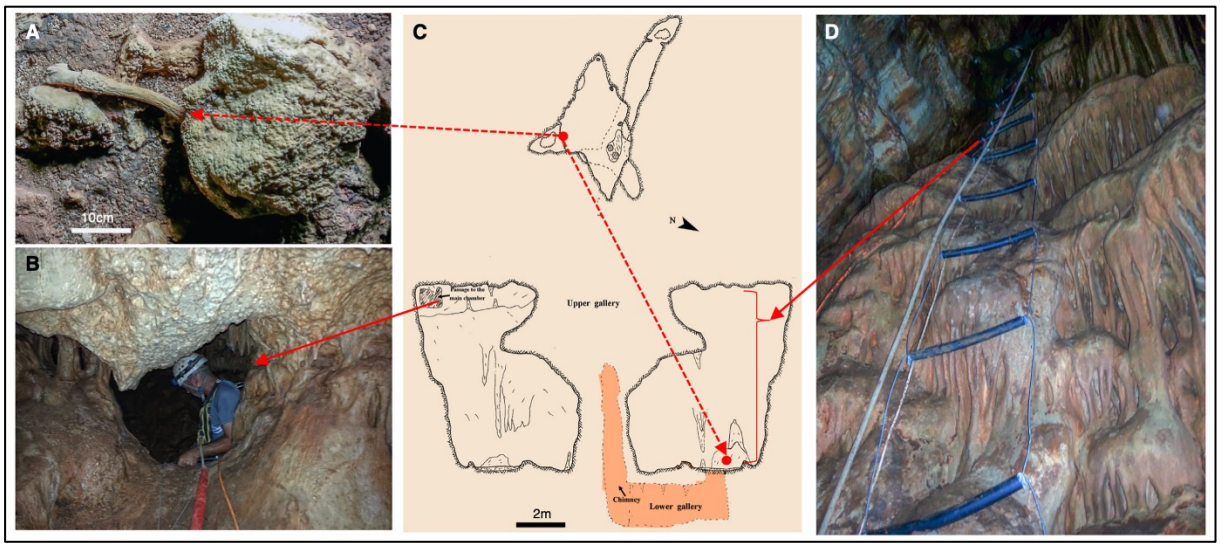

***A**. A Persian fallow deer antler recovered from the floor of the hidden chamber (Area K)**, B**. The small opening to the hidden chamber at the upper space, **C.** Schematic illustrations of the chamber, the upper illustration is a cross-section. The red dot denotes the location of the antler, **D.** Curtain of stalagmite forming the external wall of the hidden chamber.*

Area K – the "hidden chamber"

Area K is located in the south chamber, southwest of Area A, and behind a natural curtain of stalagmites (Fig. S4). The southern chamber, discovered in 2012, is composed of two small galleries: upper and lower (Fig. S4). Current access to this chamber is difficult and requires climbing to the top of the stalagmite curtain (3 m), crawling through a small tunnel (ca. 0.5 m in diameter), and rappelling down into the upper space (7 m) (Fig. S4: b, d). The upper space is almost devoid of sediments and contains very few artifacts. Notably, a complete antler of Persian fallow deer (*Dama Mesopotamica)* was found attached by flowstone to the floor of this chamber (Fig. S4a).

3. The engraved boulder

The engraved boulder, composed of dolomite, was discovered at Area H during the 2013 season (Fig. S5). Positioned within a niche along the northern wall in the cave's easternmost section (Fig. S5a), the boulder overlooks a broad horizontal expanse on an elevated surface, bordered by the bases of the

western and eastern talus (Fig. S5b). Comprehensive onsite documentation of the boulder and its surroundings was conducted using 3D scanner, as depicted in the attached photogrammetry model (**Movie. *The ritual compound and the engraved boulder from Manot Cave***).

The boulder is 5cm from the wall at the top and extends to 10cm at the base (Fig. S5c- e). Adjacent to the boulder, numerous rocks of diverse shapes and sizes line the cave wall, although none match or surpass the size of the carved boulder (Fig. S5c). Among these rocks are weathered fragments that have fallen from the cave's wall. Opposite the boulder, at a distance from the wall to the west, there is a small area nearly devoid of any additional rocks (Area A). The arrangement of the various stones surrounding the carved boulder appears to lack any discernible order or design.

The dolomite boulder displays a brown-gray color with yellow patches and gray-white stains (Fig. S6). It is 27- 29 cm in length, 20-22 cm in width (at the base), 25 cm in height (at the back), and has a weight of 28 kg (Fig. S7). The boulder, generally globular in shape, features numerous grooves that form geometric patterns on its superior (upper) face (Fig. S7a, e). The back (northern face) and the base are flat and devoid of artificial grooves (Fig. S7c, d). The lateral faces exhibit few natural shallow lines that were used as a control group in the shape analysis. The grooves on the upper (superior) face form a complex pattern, incorporating straight and curved lines (Figs. S5c, S6a, c, d, S7a, e). The back (northern face) of the boulder is slightly concave, oriented toward the cave's wall (Fig. S7c). The left (western) face stands vertically and forms a right angle with the upper-back surface of the boulder (Fig. S7b). The right face (eastern aspect) is rounded, featuring a continuous line starting from the left face and curving to meet the protruding extension on the right. Both, the upper and eastern faces are rounded, sloping from the back to the front.

The faces of the boulder are engraved in an intricate arrangement of straight and curved lines, creating a complex pattern (Fig. S7a, e). The lines are uniformly carved in the boulder, with varying widths between 2-10mm, and depths between 2-10mm (some grooves are filled with crust, affecting the measurement). Some lines continue from one face to another, some are horizontal, and some end abruptly without connecting to other grooves. It is important to note that the back of the boulder

(northern face), which faces the wall, is uncarved. The grooves extend to the protruding extension on the right end (eastern aspect), contributing to the overall pattern of the boulder.

Figure S5. The layout of Manot Cave illustrates the retrieval of the engraved boulder at Area H.

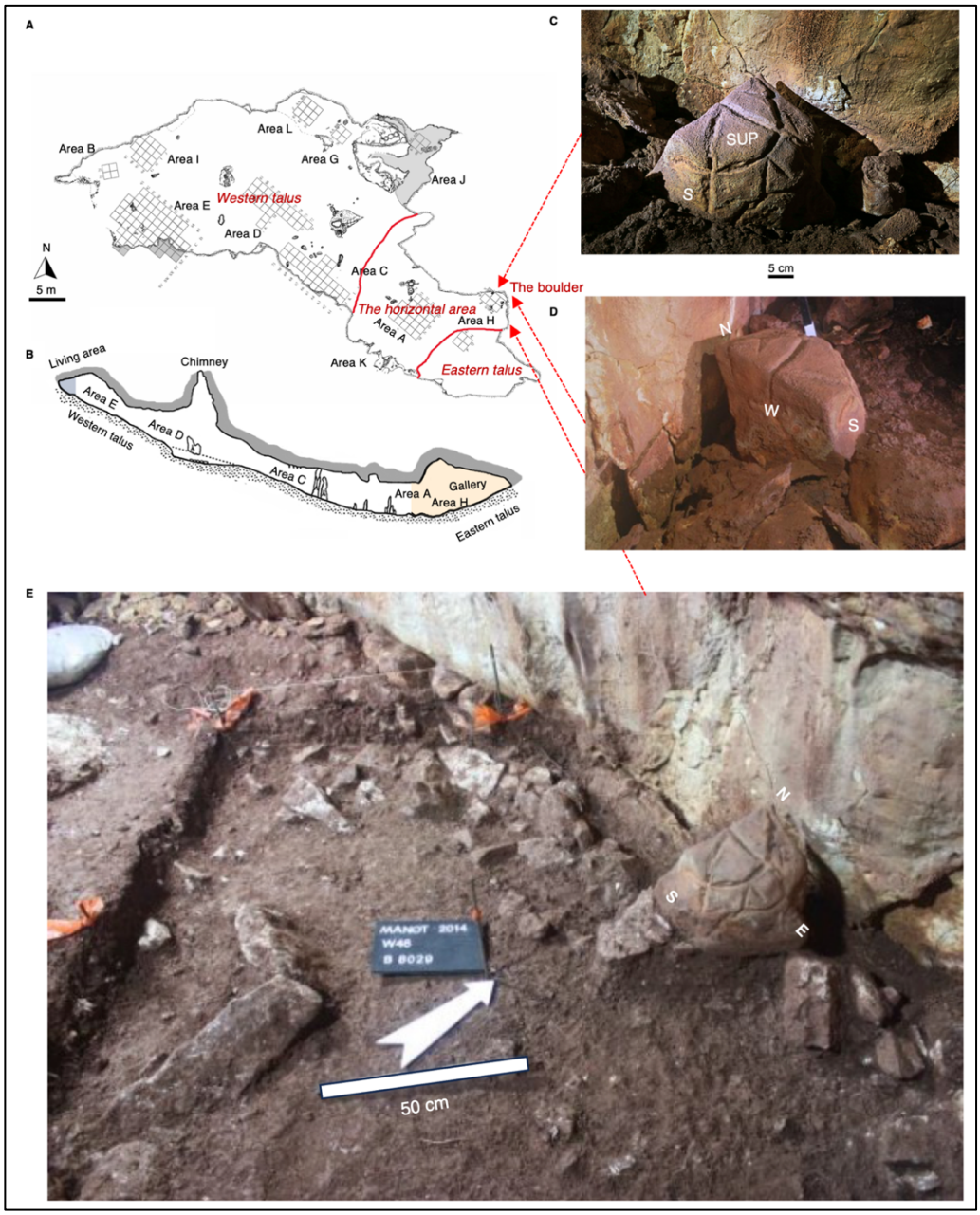

A. *Overview of the cave with excavation areas indicating the boulder's location in the inner part of the cave;* ***B****. Cross-section of the cave;* ***C****. View of the dolomite engraved boulder from southeast to northwest;* ***D****. The left side of the boulder (western face). Note that the continuous lines are also present on the top (upper face) of the boulder;* ***E****. Area H: Excavated squares surrounding the incised boulder. W-west face, E-eastern face, N-northern face, S-southern face, Sup-superior (upper) face.*

Apart from the grooves, several round holes, with a diameter of up to 20mm and a depth of 10mm, are present on the boulder (Fig S7d, S8a). These holes possibly suggest drilling activities, yet there is no apparent observation regarding their specific placement or their connection to the grooves.

Figure S6. The engraved boulder and the worked antler from different views.

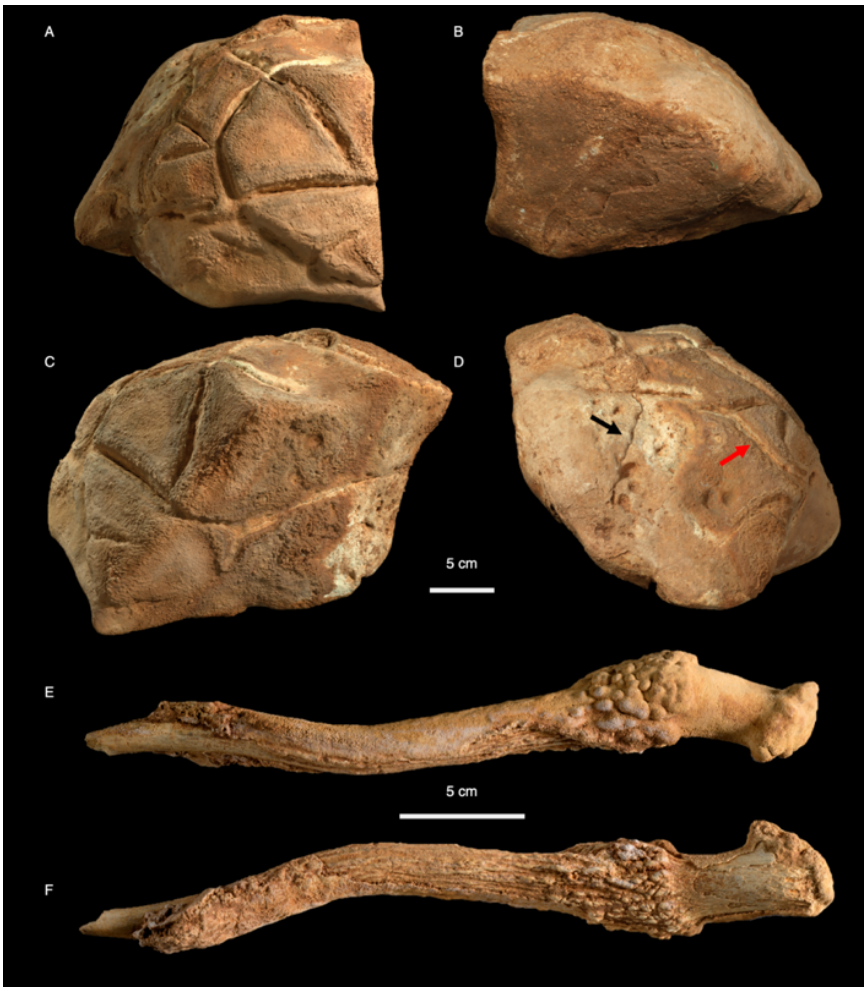

A-D. *Different views of the engraved boulder that was uncovered in the ritual compound (Area H). The grooves are located on the globular, upper aspect of the stone. The differences in shape and size between artificial grooves (red arrow) and natural grooves (black arrow) are clearly visible in D.* ***E-F.*** *Dorsal and ventral views of a Persian fallow deer (Dama mesopotamica) antler, found in the 'hidden room' (Area K). The antler is partially covered with crust, especially above the burr.*

The collective pattern of the grooves, along with the boulder's shape, closely resembles that of a tortoise's shell (see below). The substantial weight of the boulder (28 kg), along with its strategic positioning, rules out any chance occurrence – it did not roll into place due to gravity, and it was not

easy to relocate it from one place to another. Positioned above the bottom of the cave, it could not have originated from the large western talus. Placed separately from the eastern talus, on a flat and elevated surface, it aligns neatly against the wall, with its only uncarved side facing the wall. These factors strongly suggest a deliberate and strategic placement of the boulder in this particular location.

It is challenging to ascertain whether the boulder was carved *in situ* or transported from elsewhere. Carving it on the spot seems unlikely, especially considering that certain lines, particularly those on the back side of the protruding extension, would require better access and handling than is currently possible in its upright position. The boulder's proximity to the cave corner with standing active stalagmites (63) suggests an intentional choice of placement.

Figure S7. The various faces of the engraved boulder and the length of the different grooves studied.

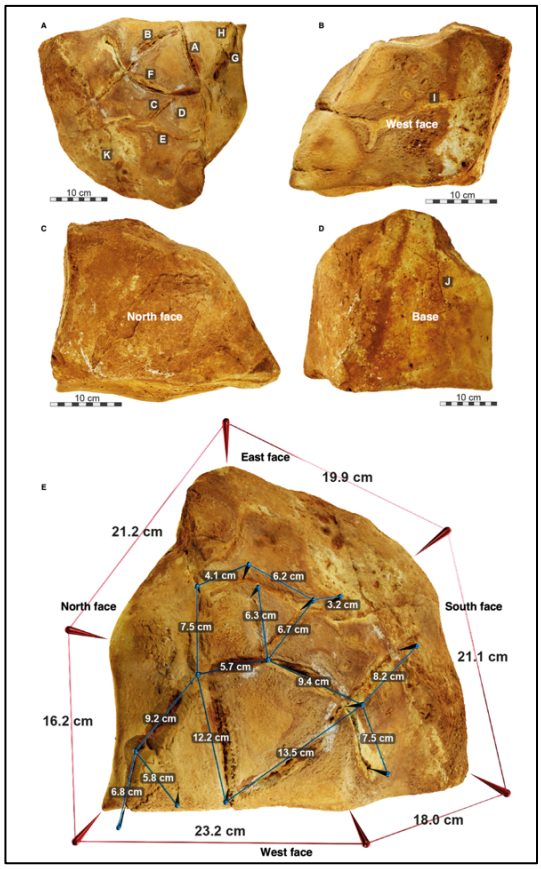

A. *Superior view of the boulder, A-K denote the grooves studied;* ***B****. The boulder's western face;* ***C****. The back of the boulder (northern face), the region that faces the cave wall;* ***D****. The base of the boulder;* ***E****. The lengths of the different measured grooves. Artificial grooves are seen mainly on the superior (upper) face of the boulder, whereas natural grooves are found on all faces of the boulder.*

4. Groove shape analysis and micro-scratches

To assess whether the grooves are natural or human-made, we conducted a 3D digital analysis of the engraving on the boulder, comparing it to the experimental engraving. The morphological analysis of the pattern relied on a high-resolution 3D model generated using a structured light scanner at the National Laboratory for Digital Documentation and Research at the Israel Antiquities Authority (76). This type of 3D model provides a detailed representation of the boulder (Fig. S8a), allowing for further investigation through computational and mathematical methods.

Our approach involved analyzing and comparing the morphology of the grooved pattern using topographic cross-sections of the boulder's surface. These cross-sections were computed from the 3D model perpendicular to the locality of the carved sections. In Fig. S8A, a rendered view of the boulder is presented, indicating the locations of four cross-sections, displayed in Fig. S8B. Each cross-section orientation was carefully chosen to maximize symmetry in accordance with its deepest point.

Figure S8. A rendered view of Manot Cave boulder and the examined grooves.

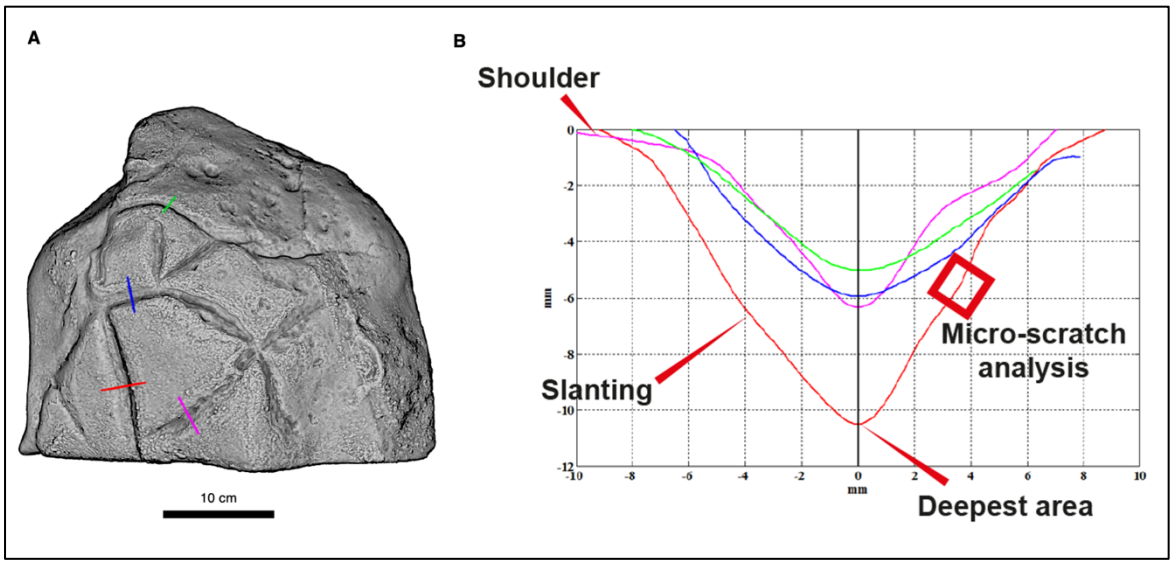

A. *The locations of the cross-sections selected on the 3D model of the boulder;* ***B.*** *The derived outlines of the profile of the grooves. The different colors indicate the location of the groove profile.*

As the superior face containing the engravings is not flat, it is essential to align all cross-sections using a standardized orientation for accurate comparisons. We opted to use the deepest point of each cross-section as the anchor point relative to which the morphology of the sections is measured and compared.

The positioning angle of the cross-sections was tilted to the point where it achieved maximum symmetry, employing the symmetry function defined by Saragusti et al. (77).

Once the adjustment of the cross-sections was established, their analysis was based on the concept of treating them as planar curves. To quantify the distance measure between every pair of cross-sections, we applied the method used by Karasik and Smilansky (76). These inner comparisons within the provided assemblage of cross-sections represent their correlations, allowing us to extract meaningful statistical groupings through cluster and principal component analyses.

We measured and analyzed the cross-sections of the grooves at 60 locations (Fig. S9). Most of these locations were strategically selected along the main grooves, as depicted in the top-left image. Additionally, some locations were selected as references and controls from other areas on the boulder, such as shallow depressions (marked as holes) or natural cracks (grooves I, J) (Fig. S9b, d).

A comprehensive approach to assessing the shapes of the topographic cross-sections entails their collective illustration and an evaluation of their overall forms. Figure S9e-j depicts the overlaps of cross-sections from six distinct grooves on the boulder, providing a visual representation for comparative analysis.

It is evident that groove A stands out as the deepest and the most prominent feature on the boulder Fig. S9a, e). Its V-shape is clearly defined, characterized by a sharp point at the bottom. While the other grooves are not as prominent, their overall V-shape is discernible, albeit less sharp at the bottom, with some exhibiting variations due to crust filling. Groove A is the exception (Fig. S9a, e), and the remaining grooves closely resemble those found on the boulder where attempts were made to replicate the pattern using modern flint tools (see paragraph below). Figure 11 illustrates the replicated grooves on this boulder and their corresponding topographic cross-sections.

A careful examination of the cross-sections presented in Fig. S8b reveals variations in their morphological characteristics. This observation suggests that the pattern on the boulder, encompassing several distinct grooves, could potentially be categorized based on the shape of these cross-sections. If indeed each groove was carved through a repetitive action with a flint tool (such as a burin, carinated end scraper, or a core following the experiment described in S.5) along its route, then different cross-

sections from the same groove should present similar shape (e.g., in terms of depth, length, angle, symmetry, etc.).

Figure S9. Four rendered views of the Manot Cave boulder showing the specific locations of the 60 cross-sections reconstructed, and the topographic cross-sections of the main grooves.

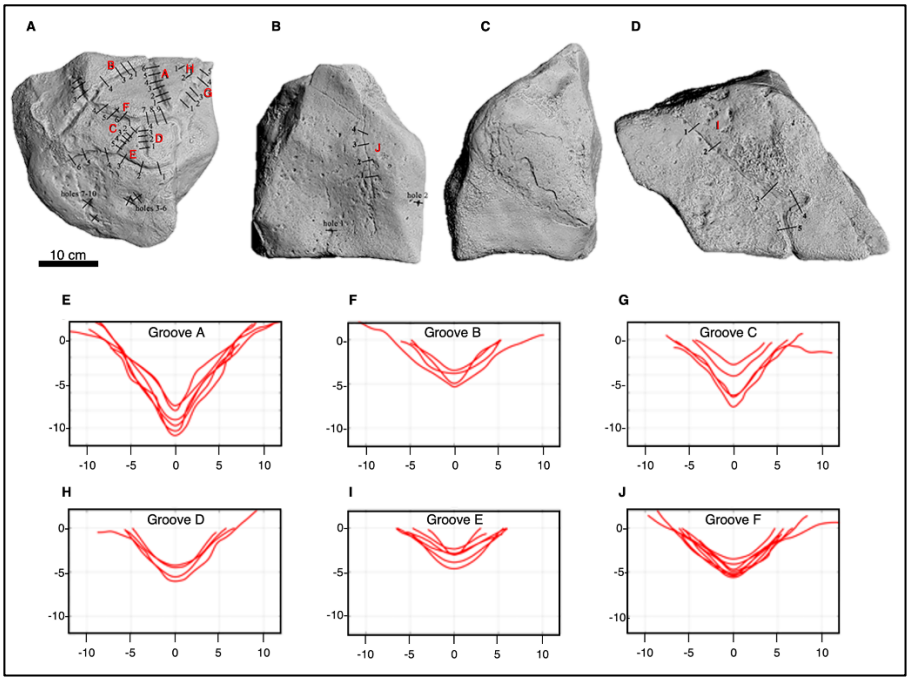

A-D. *Displaying different aspects of Manot Cave Boulder 3D scan.* ***E-J.*** *Displaying the cross-section profiles along different grooves (grooves are marked with capital letters A to J): E. at groove A, F. at groove B, G. at groove C, H. at groove D, I. at groove E, and J at groove F.*

To analyze the distinctiveness of each groove, we quantified the variations between every pair of cross-sections and employed cluster analysis to unveil internal correlations and groupings within the topographic cross-sections (Fig. S10a, b). The results are presented through a cluster tree, illustrating the hierarchical classification of the assemblage (Fig. S10c). Each leaf at the tree's bottom corresponds to a single section, with grooves identified by unique colors and symbols (Fig. S10c). Sections sharing similar morphological characteristics cluster close to each other, while those in distant branches exhibit significant differences.

The cluster-tree structure reveals two main branches, with six sub-branches. Examining the tree highlights distinct correlations between most of the grooves and their corresponding sub-branches. For

example, all six sections of groove A cluster on branch 2, with five of them grouped on sub-branch 2-a (Fig. S10c). Groove A is characterized by a straight line and is acknowledged as the deepest feature of the boulder.

Figure S10. A cluster tree of the topographic cross-sections of the grooves identified on Manot Cave boulder.

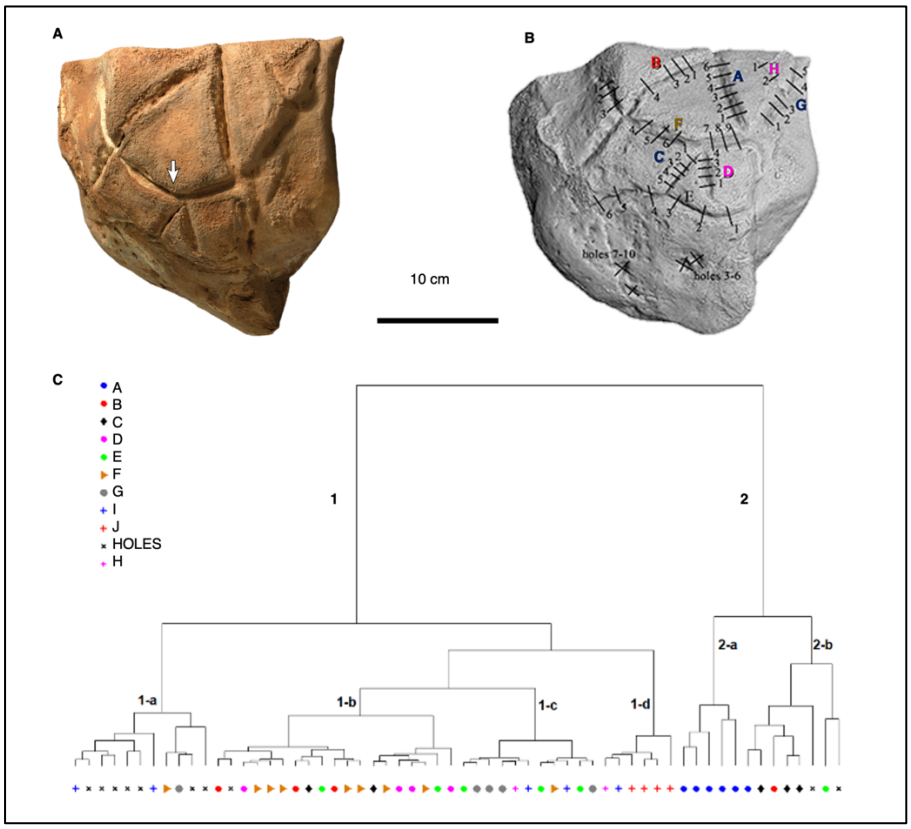

***A.** The grooves and holes on Manot Cave boulder, **B.** The grooves and holes analyzed are marked with colored capital letters (A to H). The comb-like pattern crossing the grooves marks the location of the cross-section profiles that were examined and used for statistical analysis, **C.** Cluster analysis, showing similarities in profile cross-sections among grooves.*

Adjacent to groove A, there are two deep holes (section E5 and B3) and three sections from groove C (C2, C3, C4) that were clustered on branch 2 (Fig. S10b, c). It is noteworthy that the three cross-sections that grouped with groove A are at the center of groove C (Fig. S8b), while the other two sections from that ditch, C1, and C5, are not as deep and thus classified under sub-branch 1-b (Fig. S10c). It appears that all topographic cross-sections that are less prominent than those of groove A are sorted on sub-

branch 1-b. This category includes three sections from B, two from C, all four sections of D, seven out of nine sections of F, two from E, and one gouged depression (Fig. S10c). Once again, cross-sections from the same groove tend to group together, as evident, especially for grooves B, D, and F. Similarly, the majority of groove G was classified to branch 1-c, the flat sections of groove J are on 1-d, and most cross-sections through the gouged depressions on the surface (denoted as holes) are separated on sub-branch 1-a (Fig. S10c).

Micro-scratches

To assess whether the grooves observed on the Manot Cave boulder were intentionally carved, we examined the engraved lines under a stereomicroscope. To identify micro-scratches on the beveled walls of the grooves, we utilized high-resolution replicas that facilitated the transfer of the topography of the walls of the grooves into the scanning system.

Initially, the surfaces of the walls of each groove underwent cleaning by performing multiple surface replicas (approximately 4-5) using Provil Novo Light C.D.2 silicone (Heraeus Kulzer GmbH, Dormagen, Germany). This process was repeated until the molds were free of any extraneous particles. To minimize the likelihood of surface alteration, no brushing or mechanical cleaning was conducted.

Subsequently, the surface replicas were scanned using a high-resolution disk scanning confocal microscope μsurf Explorer (NanoFocus AG, Oberhausen, Germany). Surface images were captured at a resolution of x, y = 0.16 μm and z=0.06 μm, with scans taken using a 20x objective lens to obtain 200x magnification within a total work envelope of 1.6 x 1.6 mm. Surface measurements were directly obtained from the mold and mirrored on the Z-axis using the μsoft analysis premium v. 8.0 software (NanoFocus AG, Oberhausen, Germany; a derivative of Mountains Analysis software by Digital Surf, Besancon, France). This approach allowed us to avoid an additional casting step and the potential alteration of the surface. Measurements were excluded if imperfections in the imprinting procedure were detected or if they encompassed less than 98% of the captured surface area. In such cases, scans were repeated at a slightly different location.

5. Experimental engraving

To complement the 3D analysis of the grooves, we experimentally reproduced a comparable grooved pattern on a dolomite block of similar size, using lithic flint tools (Fig. 3g). This was designed following some recent experimental studies (e.g.,(40, 78, 79). The tools are compatible with the lithic assemblages documented at the Aurignacian horizons of Manot Cave (66). These included carinated and dihedral burins, a heavy-duty scraper, and a core. The tools were handheld according to the convenience of the person who was doing the experimental carving. Following the protocol described above, surface replicas were taken, and micro-scratches analysis was done using a high-resolution disk scanning confocal microscope μsurf Explorer (NanoFocus AG, Oberhausen, Germany).

The experiment

We selected a dolomite block recovered close to the site's entrance (Fig. 3f, h). To make the grooves, we reproduced six lithic tools of different sizes (Fig. 3g). They consist of carinated and dihedral burins and a heavy-duty scraper (Tools #1-4, Fig. 3g). The lithic tools were systematically reshaped during the experiment since their working edges were worn or broken. Although we assume that the original block was engraved inside the cave, and thus in a wet condition, we engraved the boulder under both wet and dry conditions (i.e., adding water on its surface before and during the incisions), to assess the influence of the milieu in the carving.

A total of six grooves (Fig. 3h) were reproduced, creating a geometric pattern with straight incisions. The length of the grooves varies between 30-50 mm, while their width range between 2-10 mm and their depth is ca. 5-9 mm (Fig. 3d).

We initiated the experiment on a dry boulder (groove #1; Fig. S11) employing both unidirectional and bidirectional motions (approximately 65 per minute) with small and medium-sized lithic tools (tools #1-3, Fig. 3g). After about half an hour of work, we achieved only superficial incisions, and the working edges of the stone tools broke multiple times. It took over an hour to complete the groove on a dry boulder. Subsequent grooves (#2-3; Fig. 3h, j) were made with a bigger tool (tool #4, Fig. 3g) under dry conditions, yielding a similar outcome. Similarly, one hour was necessary to finish the groove, and we

had to reshape the tool's working edge every five to ten minutes. Nevertheless, using a larger flint tool resulted in a groove that was deeper and wider than the first one.

Grooves #4, 5, and 6 were crafted on a wet boulder using a single flint tool, employing the edges of this tool rather than its point (Fig. 3h, i). These conditions significantly enhanced the efficiency of carving, and after ten minutes of work, the groove was completed. To determine if this efficiency was due to the wet condition or the tool size, we alternated the procedure with a small tool (tool #3, Fig. 3g). The carving progress was slower (approximately 15 minutes) but still more efficient than under dry conditions.

The optimal combination to efficiently produce grooves on a dolomite stone appears to be on a wet boulder using a large flint tool, carving on a dry block with small tools proved to be challenging. The shape analysis of the experimented grooves reveals consistent features (e.g., all grooves were 'V'-shape in cross-section, showed denoted starting point, and exhibited flat shoulders), all also characteristic of the grooves on the boulder.

Our experiment showed that by using flint tools it is possible to reproduce an identical pattern to the one seen on the Manot Cave boulder (Fig. S11). The morphological and metrical characteristics of the experimental grooves exhibit features similar to those of the archaeological boulder, indicating that these incisions are most likely human-made rather than the result of a natural process. Furthermore, our experimental results strongly suggest that the archaeological boulder was likely worked with water. In addition, our experiment indicates that the local conditions, such as the smoothness of the boulder, the angle of the carving object, and the time invested, likely varied to some extent. Therefore, we posit that the morphological characteristics of the grooves should differ from one another, while within the same groove, these features should be consistent.

Figure S11. A typical boulder sourced from the cave area features replicated grooves, along with the topographic cross-sections of these replicated grooves.

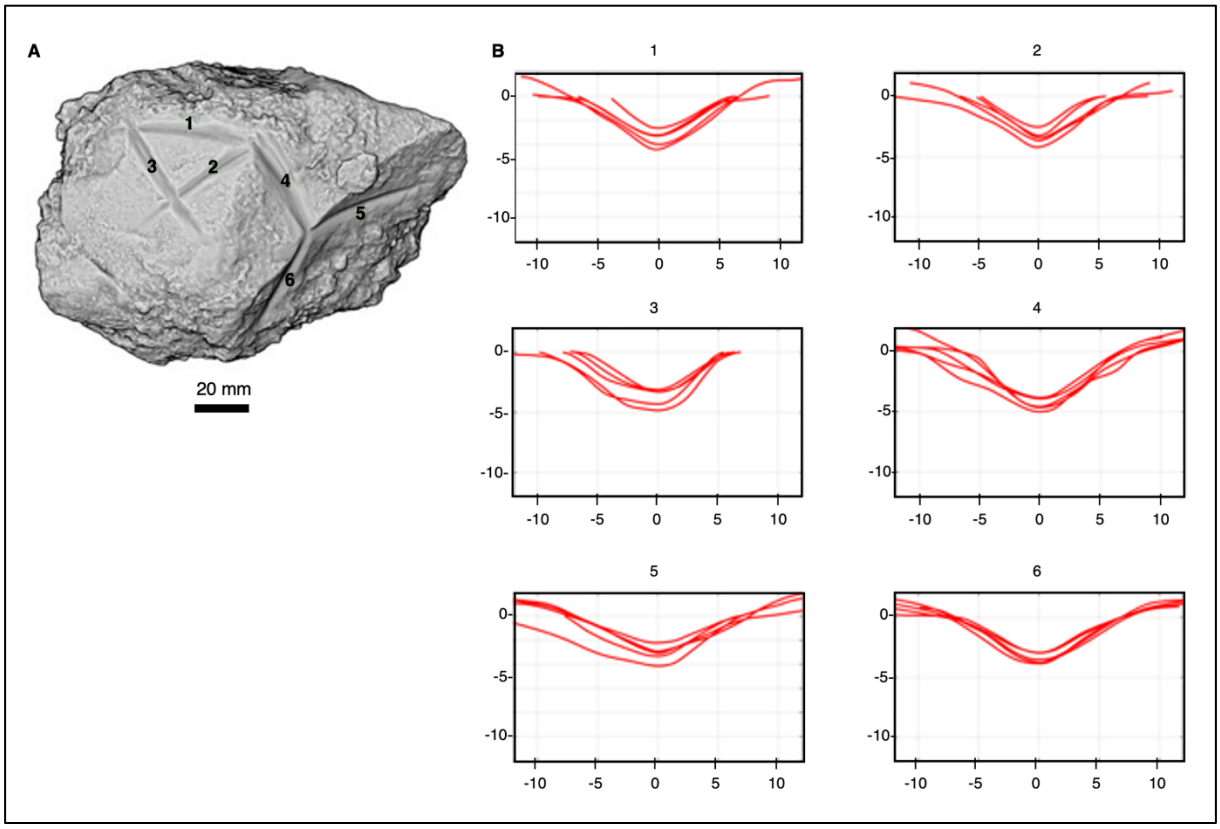

A. *The experimental replicated grooves created on a local boulder (marked with numbers 1 to 6);* ***B.*** *the topographic cross-section profiles of the replicated grooves. The numbers on the box match the numbers of the groove. For each groove, a series of cross-sectional profiles were created.*

6. The worked antler

Examination of the antler's surface using a portable microscope (Dino-Lite) revealed a series of incisions (Fig. S12). These incisions comprise a breakage at the distal end (potentially natural), a human-made perpendicular cutmark at the center, and additional oblique incisions at the proximal part (also human-made).

Figure S12. The antler of a Persian fallow deer (Dama mesopotamica) recovered at the hidden chamber at Manot Cave with cut marks.

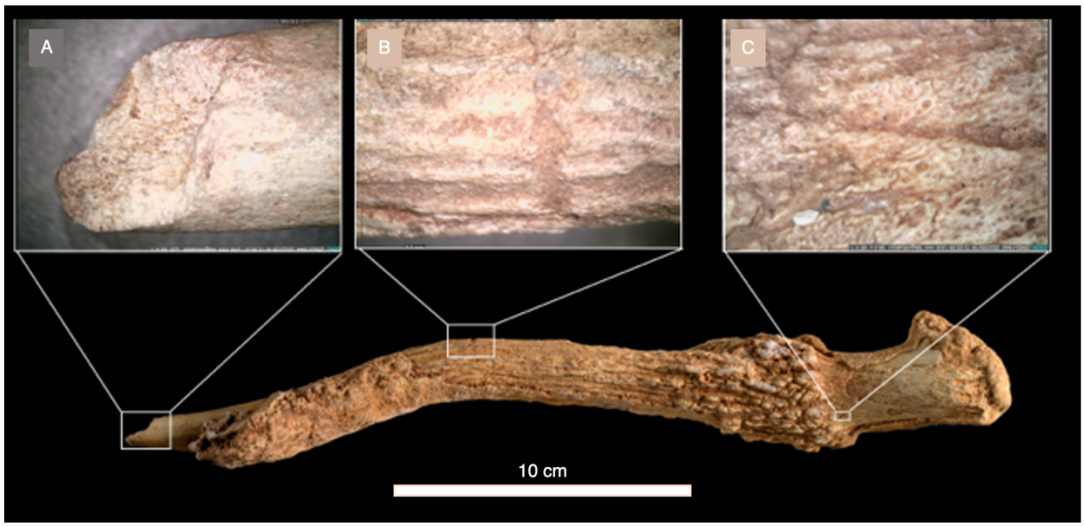

Incisions observed on the Persian fallow deer (Dama mesopotamica) antler's surface ***A.*** *Broken distal edge;* ***B.*** *Perpendicular incision;* ***C.*** *Oblique incisions.*

7. Naturally etched grooves

Condensation corrosion, a type of chemical weathering, may result from a combination of factors such as cave air composition, temperature differentials between air and rock, and the water vapor's ability to condense on bedrock and speleothems. In limestone caves, this process manifests as the etching of bedrock, impacting various pre-existing rock features through differential corrosion. These features encompass minute, often imperceptible cracks and variations in rock composition or structure. Planar fractures or fissures are common and frequently result in etched grooves, typically appearing as straight-line segments (63). These conditions and processes are ubiquitous in Manot Cave, serving as the primary natural agents that can form grooves**.**

In our investigation into the natural formation of grooves on the Manot Cave boulder, under high humidity and condensation corrosion conditions, we implemented the following steps: initially, we conducted a thorough survey of cave walls and ceiling to identify naturally etched grooves, marking their locations for subsequent study. We examined the pattern and shape of grooves generated by natural

etching and compared them with those observed on the boulder. These comparative analyses aimed to determine the potential role of natural weathering in the development of the observed grooves.

Two localities with naturally etched surfaces were identified within the cave: near the entrance and in the chimney (Fig S13a, b). While straight segments of grooves were observed on these naturally etched surfaces (Fig. S13a), they appear less distinct than those on the boulder and exhibit irregular shape and orientation.

Figure* S13. *Comparison between the pattern and shape of naturally etched grooves and artificial grooves forming geometric signs on Manot Cave boulder's surface.

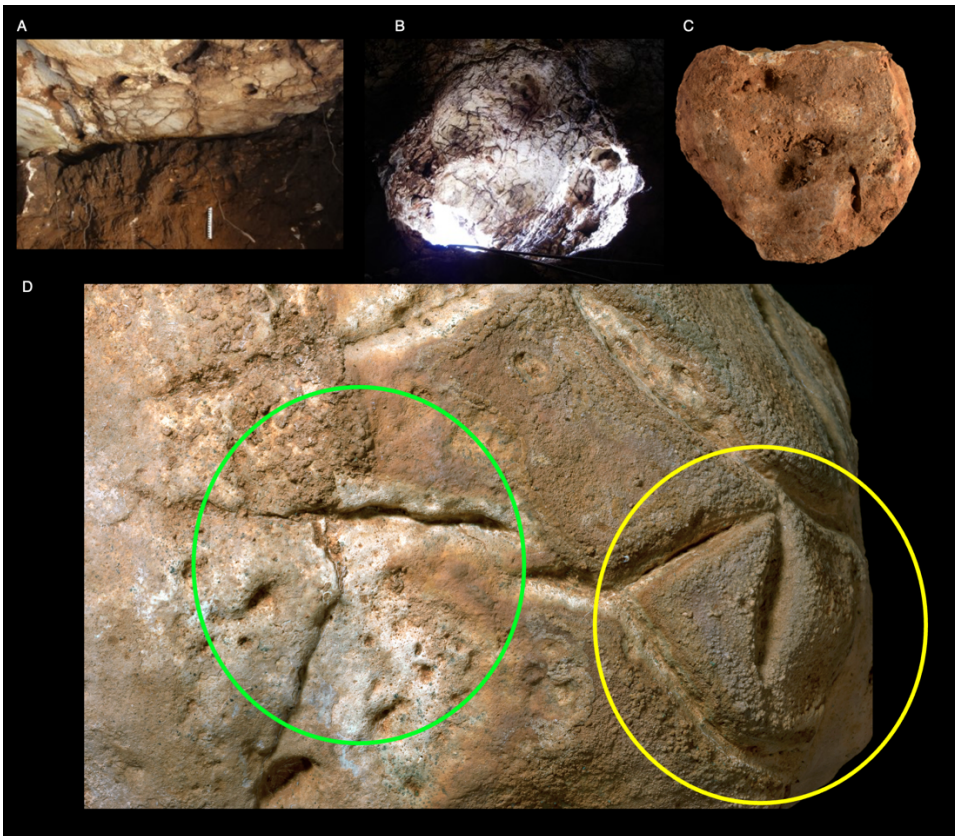

A. *Natural etchings on the ceiling of the cave adjacent to the current entrance, extending above clay colluvial filling;* ***B.*** *Etched ceiling close to the chimney. The etched grooves in this area exhibit a rough and irregular texture;* ***C.*** *A natural boulder from the deep part of the cave, devoid of any grooves;* ***D.*** *The engraved boulder shows both natural (green circle) and curved (yellow circle) grooves. The dominant geometric signs are triangular or square-shaped. The surfaces between the grooves are smooth, unlike the area between natural grooves.*

The grooves on the boulder appear comparatively more regular than those resulting from natural etching, displaying the distinctive characteristics that are discussed in the main text (e.g., starting and ending points). The lines exhibit continuity with fewer deviations than observed in natural grooves (Fig. S13a), and the surface between the individual grooves appears notably smoother than on etched surfaces (Fig. S13d).

The straight grooves on the boulder could have formed along tiny planar fissures, commonly manifested by straight lines on flat cutting surfaces. However, the presence of a curved groove makes it less likely to be associated with any fissure, and more suggestive of artificial carving. This observation implies that the associated straight grooves might also have anthropogenic origin. Further examination of other boulders of similar size from the deep part of the cave reveals an absence of grooves (Fig. S13c).

8. Dating

U-Th dating of the calcitic crust carpeting the grooves

For the purpose of U-Th dating, carbonate crust samples were drilled out from ten localities on the boulder (Fig. S14): two control samples (Fig. S14a, No. 1 and 2) were taken from the stone's surface, assuming they represent pre-engraving accumulations; seven samples (No. 3 to 9) were taken from crusts within the grooves (assuming post-engraving deposition) (Fig. S14a, b, d, No. 3 to 9); one sample (Fig. S14a, No.10) was taken from a point marking the upper end of a worked groove. The U-Th dates obtained (Fig. S14b) reveal that the grooves were created before 27.8 ka and post 59.3 ka. As expected, the older dates originate from the unworked surface of the boulder.

Approximately 0.2-0.3 g of crust from both inside and outside the grooves were drilled using 2 mm diameter diamond drill bits. The detailed dating procedure, including error statistics, is thoroughly described by Hershkovitz et al.(80) and Yasur et al.(64). Here, we provide an overview of the main features. The drilled powder was dissolved in 7M HNO3 and HF, with the addition of a 229Th/236U spike. This solution was evaporated to dryness, and the residue was re-dissolved in 4 ml of 7M HNO3. This solution was loaded onto mini-columns that contained 2 ml Bio-Rad AG 1X8 200-400 mesh resin. Uranium was eluted with 1M HBr and Th with 6M HCl into separate beakers. The U and Th beakers

were placed on a hotplate set at 215ºC, and the solutions were evaporated to complete dryness. The residues were then dissolved in 2 ml and 5 ml of 0.1M HNO3, respectively.

U-Th dating was performed using a Nu Instruments Ltd (UK) Multi-Collector-Inductively-Coupled-Plasma-Mass-Spectrometer (MC-ICP-MS) equipped with 12 Faraday cups and 3 ion counters. Each sample was introduced to the MC-ICP-MS through an Aridus® micro-concentric desolvating nebulizer sample introducing system. Instrumental mass bias was corrected (using an exponential equation) by measuring the $^{235}U/^{238}U$ ratio and correcting with the natural $^{235}U/^{238}U$ ratio.

Figure S14. Dating of the engravings on the Manot Cave boulder.

A

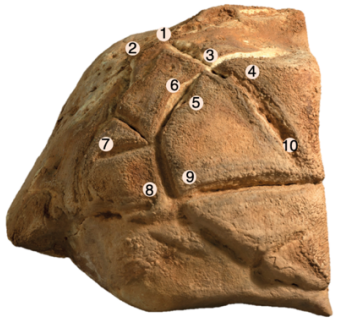

B

Sample Number	Age (ka)	Error S2
1	302.4	93.0
2	120.0	18.9
3	20.0	1.6
4	20.0	0.8
5	5.7	0.4
6	15.9	0.4
7	27.8	2.0
8	25.3	1.2
9	14.2	0.6
10	59.3	6.7

C

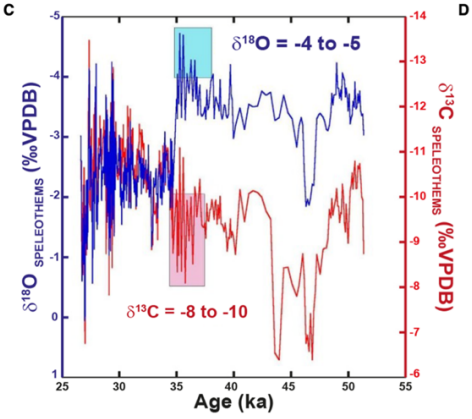

D

Sample Number	$\delta^{13}C$ ‰ (VPDB)	$\delta^{18}O$ ‰ (VPDB)
1	-8.83	-4.77
2	-9.47	-4.48
3	-8.48	-4.46
4	-9.64	-4.72
5	-7.99	-4.15
6	-8.37	-4.29
7	-9.83	-4.61
8	-9.60	-4.37
9	-9.61	-5.09
10	-9.33	-4.96
11	-9.47	-4.05

A-B. *U-Th dates of crusts sampled from various locations on the boulder: Green- from unworked boulder surface (samples 1, 2); Pink- from within the grooves (samples 3-9); Blue- from starting point of the groove (sample 10).* ***C-D.,*** *The isotopic composition of the crusts (colored rectangles) aligns with the Manot Cave speleothems (64) deposited between ~ 37-35 ka.*

VPDB=Vienna Pee Dee Belemnite

Calibration of ion counters relative to Faraday cups was performed using several cycles of measurement with different collector configurations in each specific analysis. Due to the significant amount of detrital material in the crust, all ages were corrected using a correction factor of 1.75 (80). The dating results are shown in Table S1. The error on the corrected age is in 2σ +0.15, which is the error on the correction factor (80).

Table S1. Results of the U-Th dating of the calcitic crust carpeting the grooves.

Sample No.	^{238}Uppm	error	Uncorrected ^{234}U/^{238}U	error	Corrected ^{234}U/^{238}U	error	^{230}Th/^{234}U	error	^{230}Th/^{232}Th	error	Uncorrected age (ka)	Corrected age (using Th/U=4)ka	2sigma+ /-0.15ka
T-1A	2.4137	0.0016	1.0033	0.0011	1.0033	0.0011	0.9724	0.0052	3.24	0.02	386.1	302.4	42.5
T-2	1.7115	0.0014	1.0016	0.0024	1.0016	0.0024	0.8235	0.0071	3.17	0.03	188.4	120.0	9.4
T-3	6.2702	0.0051	0.8642	0.0016	0.8642	0.0016	0.2284	0.0011	5.58	0.03	28.4	20.0	1.0
T-4	6.2510	0.0148	1.0029	0.0022	1.0029	0.0022	0.2324	0.0014	5.48	0.03	28.8	20.0	0.5
T-5	5.4604	0.0084	0.9985	0.0018	0.9985	0.0018	0.0969	0.0009	3.64	0.03	11.1	5.7	0.4
T-6	5.4005	0.0048	1.0084	0.0015	1.0084	0.0015	0.1877	0.0008	5.61	0.03	22.6	15.9	0.4
T-7	5.1230	0.0051	1.0116	0.0023	1.0116	0.0023	0.3327	0.0014	4.34	0.02	44.0	27.8	1.2
T-8	3.9915	0.0061	1.0157	0.0026	1.0157	0.0026	0.3382	0.0017	3.69	0.02	44.8	25.3	0.7
T-9	4.4232	0.0041	1.0157	0.0021	1.0157	0.0015	0.2361	0.0011	3.28	0.02	29.3	14.2	0.5
T-10	3.6145	0.0042	1.0169	0.0015	1.0169	0.0015	0.6484	0.0053	2.96	0.03	113.2	59.3	3.5

9. Stable Isotope Analysis

Stable oxygen and carbon isotope analyses were conducted following the procedure described by Yasur et al. (64). Oxygen ($\delta^{18}O$) and Carbon ($\delta^{13}C$) values of the crust were determined using approximately 0.5 mg samples (n=10) obtained from various engravings (Fig.S14c).

Dry phosphoric acid (100%) was added into the vials, initially positioned horizontally, to prevent reaction with the carbonate. Subsequently, the samples were flushed with pure helium gas for ten minutes to eliminate all atmospheric CO_2. Next, the vials were rotated to a vertical position, allowing the phosphoric acid to react with the powder of the drilled samples, forming CO_2. The CO_2 was then analyzed for $\delta^{18}O$ and $\delta^{13}C$ using a Gas Bench automatic sampler attached to a Delta V Isotope Ratio Mass Spectrometer (IRMS). All $\delta^{18}O$ and $\delta^{13}C$ values were calibrated against the international standards NBS-18 and NBS-19 and are reported in permil (‰) relative to the VPDB standard. Analytical reproducibility of duplicates is better than 0.1‰ for both $\delta^{18}O$ and $\delta^{13}C$**.**

10. Identifying carbon-rich particles in laminae of stalagmites

Thin slices (1x1 cm) of stalagmites were sawed, and the exposed lamina were examined by Environmental Scanning Electron Microscope (ESEM) Quanta-450. Back Scattered (BSE) and

Secondary Electron (SE) images were obtained, and the composition of the darker particles was determined by an Energy Dispersive Spectrometer (EDS).

Figure S15. Analysis of stalagmites at different locations in the cave to identify the presence of fire.

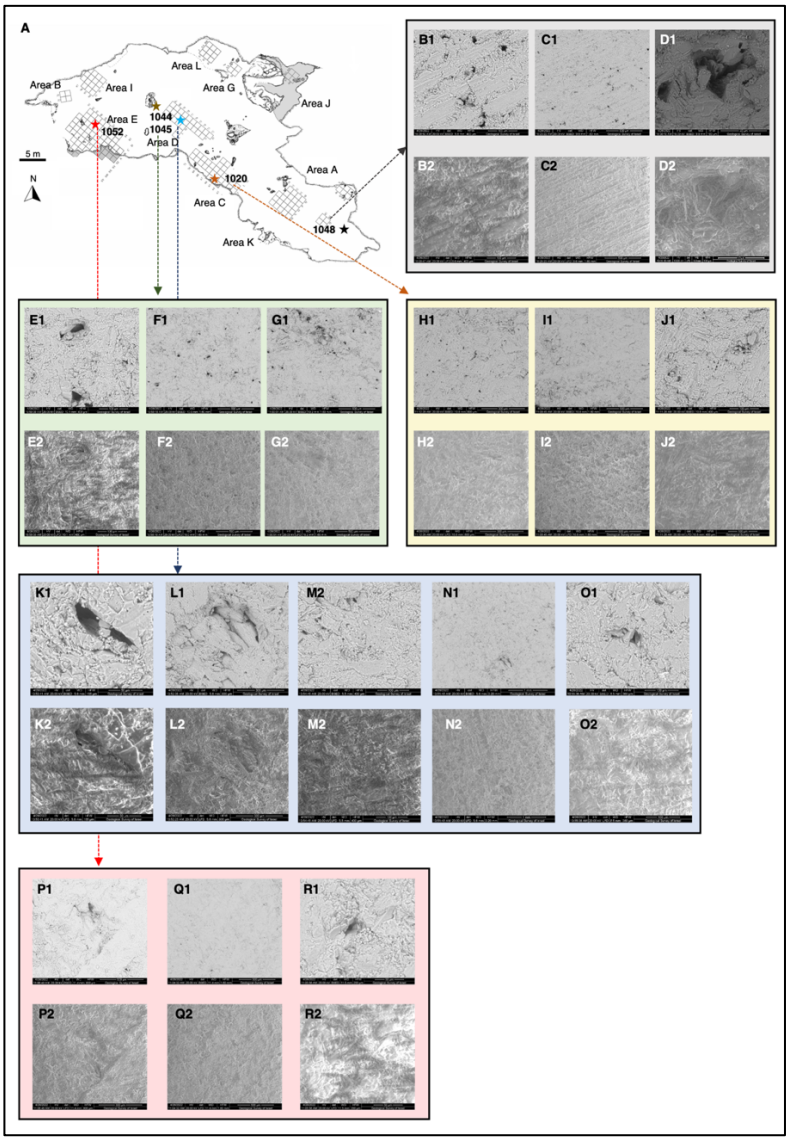

A. *Map of the cave displaying the localities of the studied stalagmites. (**Gray B-D**) Stalagmite 1048-D4 from Area A (48 ka), (**Green E-G**) Stalagmite 1045 from Area D (31-34 ka), Stalagmite 1020-C2 (**Yellow H-J**) from Area C (ca. 30 ka), (**Blue K-O**) Stalagmite 1044-A from Area D (29-30 ka), (**Pink P-R**) Stalagmite 1052 from Area E (34 ka). Environmental Scanning Electron Microscope (ESEM) images: Back Scattered Electrons image (BSE) (top line) and Secondary Electron (SE) image of the same particles (bottom line). No organic matter is observed in any of these stalagmites nor in an older lamina (48 ka) of Stalagmite 1048-A.*

The stalagmite from Area A (sample 1048; the entrance to the ritual compound) revealed evidence of dark, rounded carbon-rich particles (soot) (as determined by EDS). These particles within the stalagmite's matrix were exclusively detected in the lamina dated to ca. 36 ka, with no such spots in the older lamina (48 ka) of Stalagmite 1048 (Fig. 4). Moreover, no organic matter was observed in any of the other four stalagmites collected in various parts of the cave (Fig. S15).

11. Tortoise remains at Manot Cave and other Levantine prehistoric sites

Two chelonian species were present in the late Pleistocene Levant: the spur-thighed tortoise (*Testudo graeca*) and the Western Caspian Turtle (*Mauremys rivulata*). Among these, the spur-thighed tortoise (*Testudo graeca*), a terrestrial species that inhabits semi-arid to Mediterranean areas, dominates the zooarchaeological record (81). It also possesses a high dome-shaped carapace that is reminiscent of the Manot Cave interior space (Fig. S16), in contrast to the flatter and more elongated carapace of the freshwater turtle.

The tortoises' slowness made them a favorite catch in some Levantine Paleolithic sites (82, 83). However, their abundance in the Mediterranean southern Levant sequence exhibited notable temporal and spatial variations (Fig. S16). Unequivocal examples of tortoise collection and exploitation include a late Lower Paleolithic case (84), several Middle Paleolithic cave sites (82, 85, 86), and an open-air campsite (87).

In the Early UP, tortoises are present in small numbers. Specifically, in the Manot Ahmarian, tortoises make up 2% of the Number of Identified Species (NISP) and 3% of the NISP in the Levantine Aurignacian layer (Fig. S16). It is unclear why tortoises were collected in such low numbers by Early UP groups (71). The proportion of tortoises in Late UP and Early Epipaleolithic faunas varies, reaching more than 30% in open-air sites such as Ohalo-II (88) (Fig. S16). In the late Epipaleolithic Natufian culture, tortoises are abundant in most sites, sometimes comprising one-third of NISP (e.g., (89-92).

Tortoise remains in Natufian assemblages commonly exhibit signs of cooking, butchery, and processing marks (89-91, 93, 94), and their shells may have been used as containers (95). They are typically found as isolated limb bones, carapace, and plastron fragments. Still, several occasions of complete or near-

complete shells are known, both in living surfaces and structures (96) and within human interments (97, 98).

Figure S16. Tortoise symbolism and representation in the Paleolithic.

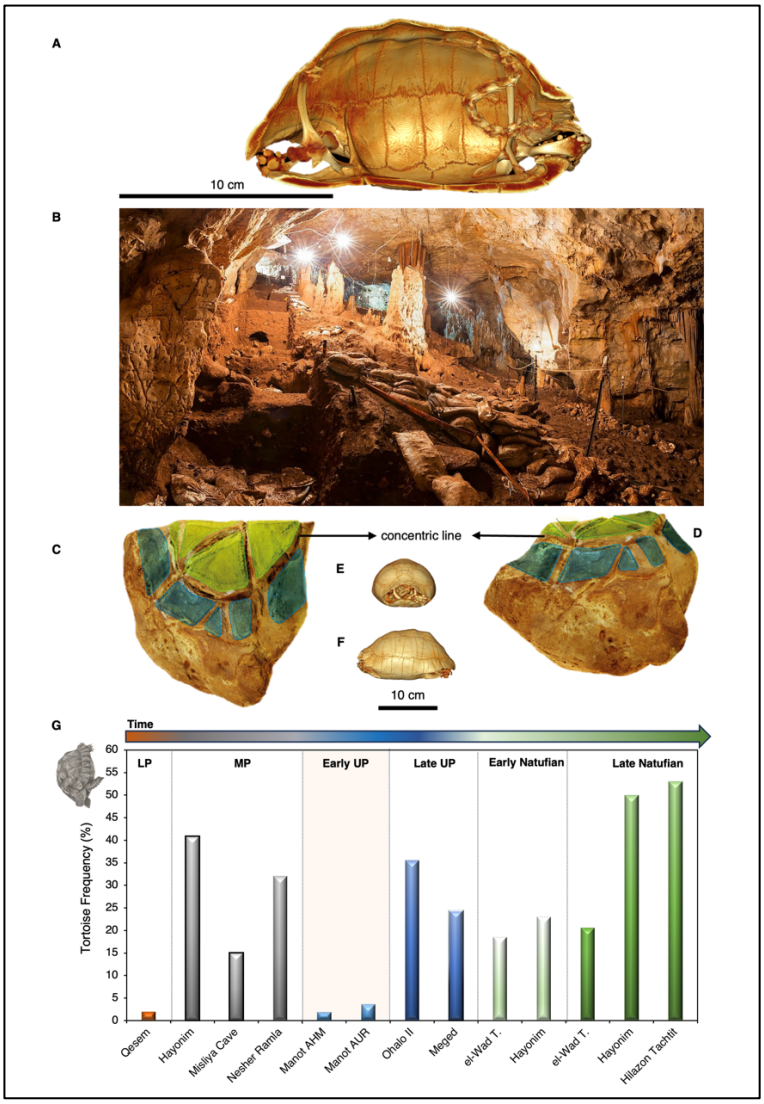

A. *Interior view of tortoise (Testudo graeca) shell (via mCT volume renderings),* ***B.*** *Manot Cave interior space;* ***C-D.*** *The engraved boulder; The geometric signs (marked by dark and light green) are arranged in two levels following the globular shape of the boulder. Note the central concentric lines separating the two 'levels' of the geometric signs on the boulder surface and the circular line in the tortoise shell separating two rows of scutes (****E-F****);* ***G.*** *Relative abundance of Mediterranean land tortoise (Testudo graeca) in Levantine prehistoric sites, by period. The tortoise relative abundance was calculated out of the NISP (all identified ungulate, bird, hare, and tortoise specimens) from representative sites of different periods (71, 82, 84, 87-90, 92, 93, 98-100): Lower Paleolithic (LP), Middle Paleolithic (MP), Upper Paleolithic (UP), Early and Late Natufian.*

A notable example is the burial of an elderly woman with numerous complete carapaces, interpreted as the remains of funerary feasts. The interred woman was interpreted as a shaman due to the ritual connection with tortoises and other animals (92, 98).

Despite differences in size and a temporal gap of approximately 12,000 years, the engraved geometric pattern on the Manot Cave boulder exhibits a striking similarity to the engraved "chevron plaquette" discovered in Kebaran contexts (ca. 25,000-23,000 years cal BP) at the Epipaleolithic site of Ein Qashish South near Mount Carmel (101, 102) (Fig. S17). Both the biological and cultural data testify to the importance of tortoises to the Levantine prehistoric people.

Figure S17. Tortoise representation in Manot Cave (UP) and Ein Qashish south (Epipaleolithic).

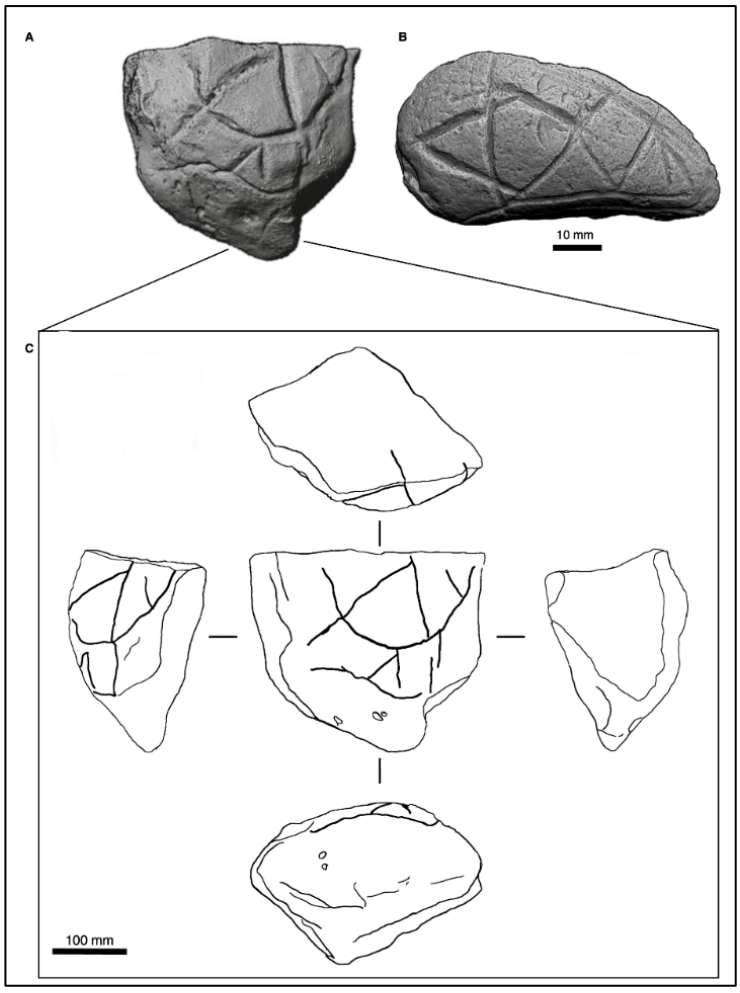

A. *Tortoise representation in engraved objects from Manot Cave; and* ***B.*** *in Ein Qashish south (Epipaleolithic) (101);* ***C.*** *Schematic drawings showing the grooves on different aspects of Manot Cave boulder. Note that the base and side walls of Manot Cave boulder are void of grooves.*

11. SI References

1. P. G. Bahn, *The Cambridge Illustrated History of Prehistoric Art* (Cambridge University press, 1998).
2. E. Dutkiewicz, G. Russo, S. Lee, C. Bentz, SignBase, a collection of geometric signs on mobile objects in the Paleolithic. *Sci. Data* **7**, 364 (2020).
3. M. García-Diez *et al.*, Visiting Palaeolithic art–explorations and archaeological implications in Cueva de las Monedas, Spain. *Oxford J. Archaeol.* **40**, 309–322 (2021).
4. A. W. G. Pike *et al.*, U-Series dating of Paleolithic art in 11 caves in Spain. *Science* **336**, 1409-1413 (2012).
5. J. Zilhão *et al.*, The rock art of the Côa Valley (Portugal) and its archaeological context: First results of current research. *Eur. J. Archaeol.* **5**, 7–49 (1997).
6. A. A. Oktaviana *et al.*, Narrative cave art in Indonesia by 51,200 years ago. *Nature*, 1–5 (2024).
7. M. Aubert, A review of rock art dating in the Kimberley, Western Australia. *J. Archaeol. Sci.* **39**, 573-577 (2012).
8. A. Brumm *et al.*, Scratching the surface: Engraved cortex as portable art in Pleistocene Sulawesi. *J. Arch. Method Th.* **27**, 670–698 (2020).
9. A. Brumm *et al.*, Oldest cave art found in Sulawesi. *Sci. Adv.* **7**, eabd4648 (2021).
10. M. Aubert *et al.*, Pleistocene cave art from Sulawesi, Indonesia. *Nature* **514**, 223–227 (2014).
11. K. Mulvaney, Iconic imagery: Pleistocene rock art development across northern Australia. *Quat. Intl.* **285**, 99–110 (2013).
12. A. Marshack, A Middle Paleolithic symbolic composition from the Golan Heights: The earliest known depictive image. *Curr. Anthropol.***37**, 357–365 (1996).
13. A. Marshack, The Berekhat Ram figurine: A late Acheulian carving from the Middle East. *Antiquity* **71**, 327–337 (1997).
14. A. Marshack, *The Roots of Civilization* (Weidenfeld and Nicolson, London, 1972).
15. A. Marshack, Cognitive aspects of Upper Paleolithic engraving. *Curr. Anthropol.***13**, 445–477 (1972).
16. F. d'Errico *et al.*, Archaeological evidence for the emergence of language, symbolism, and music–An alternative multidisciplinary perspective. *J. World Prehist.* **17**, 1–70 (2003).
17. J. Zilhão, The emergence of ornaments and art: An archaeological perspective on the origins of "Behavioral Modernity". *J. Archaeol. Res.* **15**, 1–54 (2007).
18. C. Henshilwood, "Origins of Symbolic Behaviour " in Year Book of Science and Technology. (McGraw-Hill, California, USA, 2014).
19. O. Blanca, M. García-Diez, I. Domingo, A. Martins, Dating Iberian prehistoric rock art: Methods, sampling, data, limits and interpretations. *Quat. Intl.* **572**, 88–105 (2021).

20. M. García-Diez, "'Art': Neanderthal Symbolic Graphic Behaviour" in Updating Neanderthals: Understanding Behavioural Complexity in the Late Middle Palaeolithic*,* F. Romagnoli, F. Rivals, S. Benazzi, Eds. (Elsevier, 2022), chap. 13, pp. 251–260.
21. H. Moyes, Ed., *Sacred Darkness: A Global Perspective on the Ritual Use of Caves* (University Press of Colorado, Colorado, USA, 2012), p 520.
22. A. Brumm *et al.*, Early human symbolic behavior in the Late Pleistocene of Wallacea. *Proc. Nat. Acad. Sci.* **114**, 4105–4110 (2017).
23. M. Aubert *et al.*, Earliest hunting scene in prehistoric art. *Nature* **576**, 442–445 (2019).
24. N. Goren-Inbar, A figurine from the Acheulian site of Berekhat Ram. *JIPS* **19**, 7*–12* (1986).
25. R. Bednarik, G., A figurine from the African Acheulian. *Curr. Anthropol.***44**, 405–413 (2003).
26. F. d'Errico, A. Nowell, A new look at the Berekhat Ram figurine: Implications for the origins of symbolism. *Camb. Archaeol. J.* **10**, 123–167 (2000).
27. F. d'Errico, R. G. Moreno, R. F. Rifkin, Technological, elemental and colorimetric analysis of an engraved ochre fragment from the Middle Stone Age levels of Klasies River Cave 1, South Africa. *J. Archaeol. Sci.* **39**, 942-–952 (2012).
28. C. S. Henshilwood, F. d'Errico, I. Watts, Engraved ochres from the Middle Stone Age levels at Blombos Cave, South Africa. *J. Hum. Evol.* **57**, 27–47 (2009).
29. C. S. Henshilwood *et al.*, Emergence of modern human behavior: Middle Stone Age engravings from South Africa. *Science* **295**, 1278–1280 (2002).
30. C. S. Henshilwood *et al.*, An abstract drawing from the 73,000-year-old levels at Blombos Cave, South Africa. *Nature* **562**, 115–118 (2018).
31. A. Mackay, A. Welz, Engraved ochre from a Middle Stone Age context at Klein Kliphuis in the Western Cape of South Africa. *J. Archaeol. Sci.* **35**, 1521–1532 (2008).
32. I. Watts, The pigments from Pinnacle Point Cave 13B, Western Cape, South Africa. *J. Hum. Evol.* **59**, 392–411 (2010).
33. E. Hovers, B. Vandermeersch, O. Bar-Yosef, A Middle Palaeolithic engraved artefact from Qafzeh Cave, Israel. *Rock Art Res.* **14**, 79–87 (1997).
34. O. Marder, O. Barzilai, T. Abulafia, I. Hershkovitz, M. Goder-Goldberger, "Chrono-cultural considerations of Middle Paleolithic occurrences at Manot Cave (Western Galilee), Israel" in The Middle and Upper Paleolithic Archeology of the Levant and Beyond*,* Y. Nishiaki, T. Akazawa, Eds. (Springer Singapore, Singapore, 2018), 10.1007/978-981-10-6826-3_4, pp. 49–63.
35. N. Goren-Inbar, *Quneitra—A Mousterian Site On The Golan Heights.*, Qedem (Hebrew University of Jerusalem, Jerusalem, 1990), vol. 31.
36. D. Shaham, A. Belfer-Cohen, R. Rabinovich, N. Goren-Inbar, A Mousterian engraved bone: Principles of perception in Middle Paleolithic art. *Curr. Anthropol.***60**, 708–716 (2019).

37. M. Prévost, I. Groman-Yaroslavski, K. M. Crater Gershtein, J.-M. Tejero, Y. Zaidner, Early evidence for symbolic behavior in the Levantine Middle Paleolithic: A 120 ka old engraved aurochs bone shaft from the open-air site of Nesher Ramla, Israel. *Quat. Intl.* **624**, 80–93 (2022).
38. A. Majkić, F. d'Errico, S. Milošević, D. Mihailović, V. Dimitrijević, Sequential incisions on a cave bear bone from the Middle Paleolithic of Pešturina Cave, Serbia. *J. Arch. Method Th.* **25**, 69–116 (2018).
39. A. Majkić, F. d'Errico, V. Stepanchuk, Assessing the significance of Palaeolithic engraved cortexes. A case study from the Mousterian site of Kiik-Koba, Crimea. *PLos One* **13**, e0195049 (2018).
40. J. Rodríguez-Vidal *et al.*, A rock engraving made by Neanderthals in Gibraltar. *Proc. Nat. Acad. Sci.* **111**, 13301–13306 (2014).
41. L. Losaberidze, A. Zavradashvili, V. Kenkadze, Palaeolithic rock art from Mghvimevi, western Georgia. *Archaeol. Res. Asia.* **37**, 100499 (2024).
42. M. Lorblanchet, *Les Grottes Ornées de la Préhistoire: Nouveaux Regards* (Editions Errance, France, 1995).
43. R. Bourrillon, R. White, Early Aurignacian graphic arts in the Vézère Valley: In search of an identity? *Palethnologie. Archéologie et Sciences Humaines*, 118-137 (2015).
44. R. D. Guthrie, *The Nature of Paleolithic Art* (University of Chicago Press, 2005).
45. J. D. Lewis-Williams *et al.*, The signs of all times: Entoptic phenomena in Upper Palaeolithic art [and comments and reply]. *Curr. Anthropol.***29**, 201–245 (1988).
46. G. Sauvet, R. Layton, T. Lenssen-Erz, P. Taçon, A. Wlodarczyk, Thinking with animals in Upper Palaeolithic rock art. *Camb. Archaeol. J.* **19**, 319–336 (2009).
47. P. G. Bahn, J. Vertut, *Journey Through the Ice Age* (University of California Press, Berkley, USA, 1997).
48. S. Petrognani, E. Robert, Symbolic territories in pre-Magdalenian art? *Quat. Intl.* **503**, 210–220 (2019).
49. G. Sauvet, La communication graphique paléolithique (De l'analyse quantitative d'un corpus de données à son interprétation sémiologique). *L'Anthropologie* **92**, 3–15 (1988).
50. O. Fuentes, The depiction of the individual in prehistory: Human representations in Magdalenian societies. *Antiquity* **87**, 985–1000 (2013).
51. D. Leder *et al.*, A 51,000-year-old engraved bone reveals Neanderthals' capacity for symbolic behaviour. *Nat. Ecol. Evol.* **5**, 1273–1282 (2021).
52. A. Leroi-Gourhan, *Treasures of Prehistoric Art* (H. N. Abrams, 1967), pp. 543.
53. E. Anati (2007) Engraved rocks of La Ferrassie style. in *XXII Valcamonica Symposium 2007, Rock Art in the Frame of the Cultural Heritage of Humankind*, pp 37–52.
54. R. White *et al.*, Context and dating of Aurignacian vulvar representations from Abri Castanet, France. *Proc. Nat. Acad. Sci.* **109**, 8450–8455 (2012).

55. R. White *et al.*, Newly discovered Aurignacian engraved blocks from Abri Cellier: History, context and dating. *Quat. Intl.* **498**, 99–125 (2018).
56. T. G. E. Powell, *Prehistoric Art* (Thames and Hudson, London, UK, 1966), pp. 284.
57. M. Aubert *et al.*, Palaeolithic cave art in Borneo. *Nature* **564**, 254–257 (2018).
58. M. C. Langley *et al.*, Portable art from Pleistocene Sulawesi. *Nat. Hum. Behav.* **4**, 597–602 (2020).
59. A. Belfer-Cohen, O. Bar-Yosef, The Aurignacian at Hayonim Cave. *Paléorient* **7**, 19–42 (1981).
60. O. Bar-Yosef, "Symbolic expressions in later prehistory of the Levant: Why are they so few" in Beyond Art: Pleistocene Image and Symbol*,* M. W. Conkey, O. Soffer, D. Stratmann, N. G. Jablonski, Eds. (The California Academy of Sciences, San Fransisco, CA USA, 1997), vol. 23, pp. 161–187.
61. I. Gilead, The Upper Paleolithic period in the Levant. *J. World Prehist.* **5**, 105–154 (1991).
62. J.-M. Tejero, A. Belfer-Cohen, O. Bar-Yosef, V. Gutkin, R. Rabinovich, Symbolic emblems of the Levantine Aurignacians as a regional entity identifier (Hayonim Cave, Lower Galilee, Israel). *Proc. Nat. Acad. Sci.* **115**, 5145–5150 (2018).
63. A. Frumkin, O. Barzilai, I. Hershkovitz, M. Ullman, O. Marder, Karst terrain in the western upper Galilee, Israel: Speleogenesis, hydrogeology and human preference of Manot Cave. *J. Hum. Evol.* **160**, 102618 (2021).
64. G. Yasur *et al.*, Climatic and environmental conditions in the Western Galilee, during Late Middle and Upper Paleolithic periods, based on speleothems from Manot Cave, Israel. *J. Hum. Evol.* **160**, 102605 (2021).
65. F. Berna *et al.*, Site formation processes at Manot Cave, Israel: Interplay between strata accumulation in the occupation area and the talus. *J. Hum. Evol.* **160**, 102883 (2021).
66. O. Marder *et al.*, Preliminary observations on the Levantine Aurignacian sequence of Manot Cave: Cultural affiliations and regional perspectives. *J. Hum. Evol.* **160**, 102705 (2021).
67. M. Shemer *et al.*, Intra-site variability – Analysis, characterization, and cultural affiliation of the Upper Paleolithic sequence of Manot Cave (Western Galilee, Israel). *Archaeol. Res. Asia.* **37**, 1–25 (2024).
68. M. Shemer, O. Barzilai, O. Marder, Cultural dynamics in the Levantine Upper Paleolithic, ca. 40–33 ky BP: Insights based on recent advances in the study of the Levantine Aurignacian, the Arkov-Divshon, and the Atlitian. *J. Paleolit. Archaeol.* **7**, 10 (2024).
69. O. Barzilai, I. Hershkovitz, O. Marder, The early Upper Paleolithic period at Manot Cave, Western Galilee, Israel. *Hum. Evol.* **31**, 85–100 (2016).
70. O. Barzilai, O. Marder, I. Hershkovitz, In search of modern humans and the Early Upper Paleolithic at Manot Cave: An overview. *J. Hum. Evol.* **160**, 102965 (2021).

71. R. Yeshurun, N. Schneller-Pels, O. Barzilai, O. Marder, Early Upper Paleolithic subsistence in the Levant: Zooarchaeology of the Ahmarian–Aurignacian sequence at Manot Cave, Israel. *J. Hum. Evol.* **160**, 102619 (2021).

72. J.-M. Tejero *et al.*, The osseous industry from Manot Cave (Western Galilee, Israel): Technical and conceptual behaviours of bone and antler exploitation in the Levantine Aurignacian. *Quat. Intl.* **403**, 90–106 (2016).

73. T. Abulafia, M. Goder-Goldberger, F. Berna, O. Barzilai, O. Marder, A technotypological analysis of the Ahmarian and Levantine Aurignacian assemblages from Manot Cave (Area C) and the interrelation with site formation processes. *J. Hum. Evol.* **160**, 102707 (2021).

74. S. Borgel *et al.*, Early Upper Paleolithic human foot bones from Manot Cave, Israel. *J. Hum. Evol.* **160**, 102668 (2021).

75. B. Alex *et al.*, Radiocarbon chronology of Manot Cave, Israel and Upper Paleolithic dispersals. *Sci. Adv.* **3**, e1701450 (2017).

76. A. Karasik, U. Smilansky, Computerized morphological classification of ceramics. *J. Archaeol. Sci.* **38**, 2644–2657 (2011).

77. I. Saragusti, A. Karasik, I. Sharon, U. Smilansky, Quantitative analysis of shape attributes based on contours and section profiles in artifact analysis. *J. Archaeol. Sci.* **32**, 841–853 (2005).

78. M. Alvarez, D. Fiore, E. Favret, R. C. Guerra, The use of lithic artefacts for making rock at engravings: Observation and analysis of use-wear traces in experimental tools through optical microscopy and SEM. *J. Archaeol. Sci.* **28**, 457–464 (2001).

79. F. d'Errico, P. Villa, Holes and grooves: The contribution of microscopy and taphonomy to the problem of art origins. *J. Hum. Evol.* **33**, 1–31 (1997).

80. I. Hershkovitz *et al.*, Levantine cranium from Manot Cave (Israel) foreshadows the first European modern humans. *Nature* **520**, 216–219 (2015).

81. R. Biton, G. Sharon, M. Oron, T. Steiner, R. Rabinovich, Freshwater turtle or tortoise? The exploitation of Testudines at the Mousterian site of Nahal Mahanayeem Outlet, Hula Valley, Israel. *J. Archaeol. Sci. : Rep.* **14**, 409–419 (2017).

82. M. C. Stiner, *The Faunas of Hayonim Cave, Israel: A 200,000-Year Record of Paleolithic Diet, Demography, and Society* (Peabody Museum Press, Harvard University, Cambridge Massachusetts, 2005).

83. M. C. Stiner, N. D. Munro, T. A. Surovell, The tortoise and the hare: small-game use, the broad-spectrum revolution, and Paleolithic demography. *Curr. Anthropol.***41**, 39–79 (2000).

84. R. Blasco *et al.*, Tortoises as a dietary supplement: A view from the Middle Pleistocene site of Qesem Cave, Israel. *Quat. Sci. Rev.***133**, 165–182 (2016).

85. J. D. Speth, E. Tchernov, Middle Paleolithic tortoise use at Kebara Cave (Israel). *J. Archaeol. Sci.* **29**, 471–483 (2002).

86. M. C. Stiner, N. D. Munro, T. A. Surovell, E. Tchernov, O. Bar-Yosef, Paleolithic population growth pulses evidenced by small animal exploitation. *Science* **283**, 190–194 (1999).

87. K. M. Crater Gershtein, Y. Zaidner, R. Yeshurun, A campsite on the open plain: Zooarchaeology of Unit III at the Middle Paleolithic site of Nesher Ramla, Israel. *Quat. Intl.* **624**, 49–66 (2022).

88. T. Steiner, R. Biton, D. Nadel, F. Rivals, R. Rabinovich, Abundance or stress? Faunal exploitation patterns and subsistence strategies: The case study of Brush Hut 1 at Ohalo II, a submerged 23,000-year-old camp in the Sea of Galilee, Israel. *PLos One* **17**, e0262434 (2022).

89. N. D. Munro, Zooarchaeological measures of hunting pressure and occupation intensity in the Natufian: Implications for agricultural origins. *Curr. Anthropol.***45**, S5–S34 (2004).

90. R. Yeshurun, G. Bar-Oz, M. Weinstein-Evron, Intensification and sedentism in the terminal Pleistocene Natufian sequence of *el*-Wad Terrace (Israel). *J. Hum. Evol.* **70**, 16–35 (2014).

91. L. Grosman, N. Munro, The sacred and the mundane: Domestic activities at a Late Natufian burial site in the Levant. *Before Farming* **2007**, 1–14 (2007).

92. L. Grosman, N. D. Munro, A. Belfer-Cohen, A 12,000-year-old Shaman burial from the southern Levant (Israel). *Proc. Nat. Acad. Sci.* **105**, 17665–17669 (2008).

93. N. D. Munro, Small game, the Younger Dryas, and the transition to agriculture in the Southern Levant. *MGFU* **12**, 47–71 (2003).

94. M. C. Stiner, N. D. Munro, Approaches to prehistoric diet breadth, demography, and prey ranking systems in time and space. *J. Arch. Method Th.***9**, 181–214 (2002).

95. F. Lander, T. Russell, A southern African archaeological database of organic containers and materials, 800 cal BC to cal AD 1500: Possible implications for the transition from foraging to livestock-keeping. *PLos One* **15**, e0235226 (2020).

96. R. Yeshurun, G. Bar-Oz, D. Kaufman, M. Weinstein-Evron, Purpose, permanence, and perception of 14,000-year-old architecture: Contextual taphonomy of food refuse. *Curr. Anthropol.***55**, 591–618 (2014).

97. D. A. E. Garrod, D. M. A. Bate, *The Stone Age of Mount Carmel: Excavations at the Wady El-Mughara; Report of the Joint Expedition of the British School of Archaeology in Jerusalem and the American School of Prehistoric Research (1929-34).* (Clarendon Press, Oxford, UK, 1937).

98. N. D. Munro, L. Grosman, Early evidence (*ca*.12,000 B.P.) for feasting at a burial cave in Israel. *Proc. Nat. Acad. Sci.* **107**, 15362–15366 (2010).

99. R. Yeshurun, G. Bar-Oz, M. Weinstein-Evron, Modern hunting behavior in the early Middle Paleolithic: Faunal remains from Misliya Cave, Mount Carmel, Israel. *J. Hum. Evol.* **53**, 656–677 (2007).

100. S. L. Kuhn *et al.*, The last glacial maximum at Meged rockshelter, Upper Galilee, Israel. *JIPS* **34**, 5–47 (2004).

101. A. Yaroshevich *et al.*, A unique assemblage of engraved plaquettes from Ein Qashish South, Jezreel Valley, Israel: Figurative and non-figurative symbols of Late Pleistocene hunters-gatherers in the Levant. *PLos One* **11**, e0160687 (2016).
102. C. Belli *et al.*, A Late Pleistocene Eastern Mediterranean palaeoclimate record based on stable carbon isotopes (Δ13C) of archaeological charcoal: New data from the Epipalaeolithic sequence of Ein Qashish South, Israel. *J. Archaeol. Sci. : Rep.* **57**, 104597 (2024).